Cell Reports
Methods

Article

A single-shot hyperspectral phasor camera for fast, multi-color fluorescence microscopy

Graphical abstract

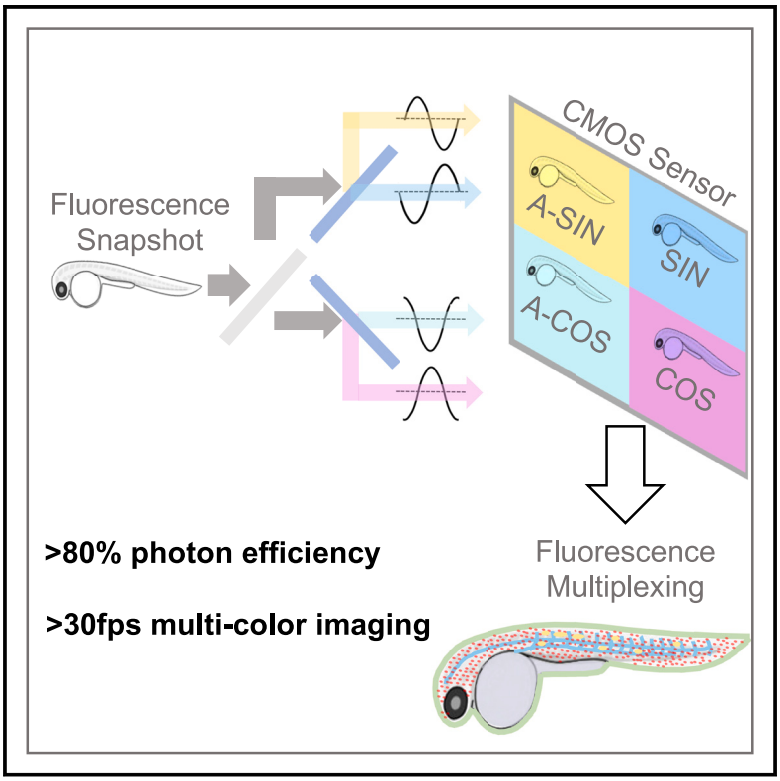

Highlights

- SHy-Cam captures fluorescence spatial and spectral information in a single exposure
- Photon efficiency of over 80% enables acquisition over 30 datasets per second
- Shy-Cam has a simple design, uses available components, and is low cost

Authors

Pu Wang, Masahiro Kitano, Kevin Keomanee-Dizon, Thai V. Truong, Scott E. Fraser, Francesco Cutrale

Correspondence

cutrale@usc.edu

In brief

Wang et al. develop single-shot hyperspectral phasor camera (SHy-Cam), a method that acquires spectral images of biological samples in a single shot with high speed and efficiency. Live imaging with SHy-Cam offers high speed and sensitivity, ease of use, and cost effectiveness, making it a valuable tool for multi-color fluorescence imaging.

Wang et al., 2023, Cell Reports Methods 3, 100441
April 24, 2023
https://doi.org/10.1016/j.crmeth.2023.100441

CellPress

Cell Reports Methods

CellPress
OPEN ACCESS

Article

A single-shot hyperspectral phasor camera for fast, multi-color fluorescence microscopy

Pu Wang,[1,2] Masahiro Kitano,[1,3] Kevin Keomanee-Dizon,[1,4] Thai V. Truong,[1,3] Scott E. Fraser,[1,2,3] and Francesco Cutrale[1,2,5,*]

[1]Translational Imaging Center, University of Southern California, 1002 West Childs Way, Los Angeles, CA 90089, USA
[2]Biomedical Engineering, University of Southern California, 1002 West Childs Way, Los Angeles, CA 90089, USA
[3]Molecular and Computational Biology, University of Southern California, 1002 West Childs Way, Los Angeles, CA 90089, USA
[4]Joseph Henry Laboratories of Physics, Princeton University, Princeton, NJ 08544, USA
[5]Lead contact
*Correspondence: cutrale@usc.edu
https://doi.org/10.1016/j.crmeth.2023.100441

MOTIVATION Observation of multiple fluorescent labels *in vivo* in biological samples at higher spatiotemporal resolution is becoming more common in biomedical research, but it is challenged by the spectral overlap between fluorescent labels. Traditional hyperspectral sampling strategies can overcome spectral overlap by permitting computational "unmixing" of the different labels, but they do so with reduced detection photon-efficiency, slowing image acquisition and increasing sample photo-bleaching and photo-toxicity. There is an unmet need for a simple, efficient, and fast spectral camera that can capture the spectral information in a single exposure, enabling full-speed volumetric fluorescent multiplexing of molecules, organelles, cells, and tissues in biological samples.

SUMMARY

Hyperspectral fluorescence imaging improves multiplexed observations of biological samples by utilizing multiple color channels across the spectral range to compensate for spectral overlap between labels. Typically, spectral resolution comes at a cost of decreased detection efficiency, which both hampers imaging speed and increases photo-toxicity to the samples. Here, we present a high-speed, high-efficiency snapshot spectral acquisition method, based on optical compression of the fluorescence spectra via Fourier transform, that overcomes the challenges of discrete spectral sampling: single-shot hyperspectral phasor camera (SHy-Cam). SHy-Cam captures fluorescence spatial and spectral information in a single exposure with a standard scientific CMOS camera, with photon efficiency of over 80%, easily and with acquisition rates exceeding 30 datasets per second, making it a powerful tool for multi-color *in vivo* imaging. Its simple design, using readily available optical components, and its easy integration provide a low-cost solution for multi-color fluorescence imaging with increased efficiency and speed.

INTRODUCTION

Hyperspectral fluorescence imaging has been gaining popularity in life sciences because of its ability to improve the selective detection of signals in specimens with significant background and to simultaneously detect multiple analytes, which increases multiplexing capability.[1–5] This advancement in fluorescence imaging is enabled by extending the image acquisition dimension into the spectral domain. Hyperspectral detection is available in commercial confocal laser-scanning microscopes (CLSMs), separating distinct spectral bands to different detectors or to different elements of detector arrays. However, inefficiency in the light path of CLSM devices, combined with the low efficiency of the detectors employed, detect a small minority of the collected fluorescence light. Furthermore, point-scanning imaging tools are not ideal for multiplexed live imaging of light-sensitive samples because of their relatively slow imaging speeds and their use of an epi-illumination path that exposes the entire depth of the specimen to the exciting light. Thus, the improved label selectivity of hyperspectral CLSMs is achieved at a significant cost in speed and photo-toxicity.

Faster and gentler wide-field imaging has been offered by approaches based on the principle of selective plane illumination microscopy (SPIM).[6,7] SPIM typically uncouples excitation and detection paths by using orthogonally oriented objectives to provide separate fluorescence excitation and detection pathways. The thin sheet of exciting light preferentially illuminates the focal plane, minimizing unnecessary excitation of fluorophores above

and below, reducing photo-bleaching and photo-toxicity. The wide-field detection permits the use of efficient (>90%) and fast scientific CMOS (sCMOS) detectors, further improving the photon budget. Higher imaging efficiency makes it feasible to perform large volumetric imaging at high spatial and temporal resolution for extended periods of time.[8,9] However, live multiplexing of fluorescent signals in SPIM has been limited by the complexity of acquiring multi-spectral datasets (3D: x, y, wavelength) efficiently on a 2D camera sensor. SPIM systems usually acquire multiple fluorescent channels sequentially using band-pass filters, which reject a significant fraction of the fluorescence emission, reducing the photon efficiency and performance of the system. Furthermore, this approach limits temporal resolution because of the need for multiple images and the time required for filter changes. Multiple exposures increase the total illumination energy load on the sample, increasing photo-toxicity. Approaches employing spectral separation of the signals[6,7] have done so at a cost to the imaging speed.

Single-exposure (snapshot) spectral acquisitions either using multiple cameras[10] or a single camera coupled with an image splitter,[11,12] as well as image mapping spectrometry (IMS),[3,5] can help decrease the temporal and photo-toxicity costs of multi-label SPIM. IMS and similar wide-field snapshot methods separate the emission light into a large number of color channels by dispersive optics so that both spectral and spatial information can be reassigned to different areas of the camera sensor acquiring a spectral cube (x, y, wavelength). The low photon efficiency of the dispersive optics (normally below 60%) combined with many narrow spectral bands[13] result in as little as ~1% of the emitted fluorescence reaching the detector in each channel. Given the limited signal intensities obtained from *in vivo* fluorescence imaging, achieving a sufficient signal-to-noise ratio (SNR) with the low sensitivity of standard snapshot hyperspectral approaches requires that exposure time and/or laser power be increased. These factors hamper temporal resolution and cause increases in photo-toxicity. For example, the fastest spectral fluorescence imaging method, SPIM IMS, is reported to require 250 ms for the snapshot acquisition, achieving 4 spectral datasets per second.[5] Such exposure times are too long for many dynamic *in vivo* imaging applications, which benefit from video of faster frame rates. A more efficient spectral sampling and compressing strategy that offers higher photon efficiency is key to achieving the needed sensitivity and speed.

Spectral phasor (SP) has proven to be an efficient and robust method for compressing and analyzing hyperspectral fluorescence datasets.[14–17] SP performs a Fourier transform on the original high-dimension hyperspectral vectors and uses the first harmonic coefficients, the so-called 2D phasor coefficients, to offer a compressed spectral representation (STAR Methods). It simplifies the interpretation and processing of high-dimension hyperspectral data and preserves most of the spectral information. The Gratton lab has integrated SP into the image acquisition step (phasor-based hyperspectral snapshot microscopy)[18,19] by collecting three images: optically sampling fluorescent emission spectra with sequentially collecting two images through distinct sinusoidal optical filters followed by another with no filters for data normalization. Compared with the traditional hyperspectral sampling with many narrow uniform color channels, each sinusoidal filter allows many more emitted photons to reach the detector (~40% efficient, for commonly used fluorescent labels), which increases SNR while maintaining reduced laser power during sensitive *in vivo* imaging. This filter-based SP method can properly and quantitatively separate more than four fluorescence signatures from multi-labeled samples.[18,19]

Any filter changing approach, including the filter-based SP approach, requires multiple exposures with intervening filter changes, limiting the temporal resolution to ~3 spectral datasets per second.[19] Photo-toxicity is increased due to the additional illumination required for multiple exposures. In addition, even with increased photon throughput efficiency, the absorption-based sinusoidal filters reject more than half of the fluorescent photons, sacrificing spectral information.[20] The method presented here, single-shot hyperspectral phasor camera (SHy-Cam), removes the need for multiple exposures, thus harvesting the advantages of the efficient SP sampling strategy with higher temporal and photon efficiency. This improved performance is validated for fluorescent imaging of live tissues in low-signal and low-SNR conditions.

RESULTS

Accessing spectral information with faster single-snapshot acquisition

Inspired by the capabilities of the Gratton lab's filter-based SP approach[18,19] and the added spectral information from the originally discarded reflected fluorescence,[20] we developed SHy-Cam. SHy-Cam is designed to fit in the detection path of wide-field microscopes and to offer hyperspectral imaging by projecting spectrally encoded channels onto a single camera sensor with a single acquisition (Figure 1). SP encoding is achieved by simultaneously capturing transmitted and reflected fluorescence emission on the camera sensor using two custom sinusoidal dichroic mirrors, folding mirrors, and lenses (Figures 1A and 1B; STAR Methods). SHy-Cam distinguishes itself from existing work[18,19] in two main aspects: speed (requiring only one single exposure to capture a spectral dataset) and photon recycling (permitting most of the collected fluorescence signal to be detected).

SHy-Cam easily achieves video speed and even faster detection (Video S4) by eliminating the need for multiple exposures and mechanical filter changes. The recycling and collection of reflected photons with SHy-Cam increase the detected spectral information[20] and provide the flexibility of spectral analysis. Ratiometric multiplexing such as spectral linear unmixing (LU)[21,22] (STAR Methods) can be applied to the four-channel data acquired with SHy-Cam, providing an addition to the standard spectral 2D phasor plane analysis (STAR Methods) shared with the filter-based SP approach.[18,19] Our results show SHy-Cam's capability of cleanly separate five fluorescence emissions with spectral LU analysis (Figures 3 and S2D–S2F).

SHy-Cam is a cost-effective and versatile add-on device for existing microscopes

SHy-Cam is designed as an add-on spectral encoding device that can be adapted to most wide-field microscopes equipped with infinity-corrected detection objective lenses. SHy-Cam

CellPress
OPEN ACCESS

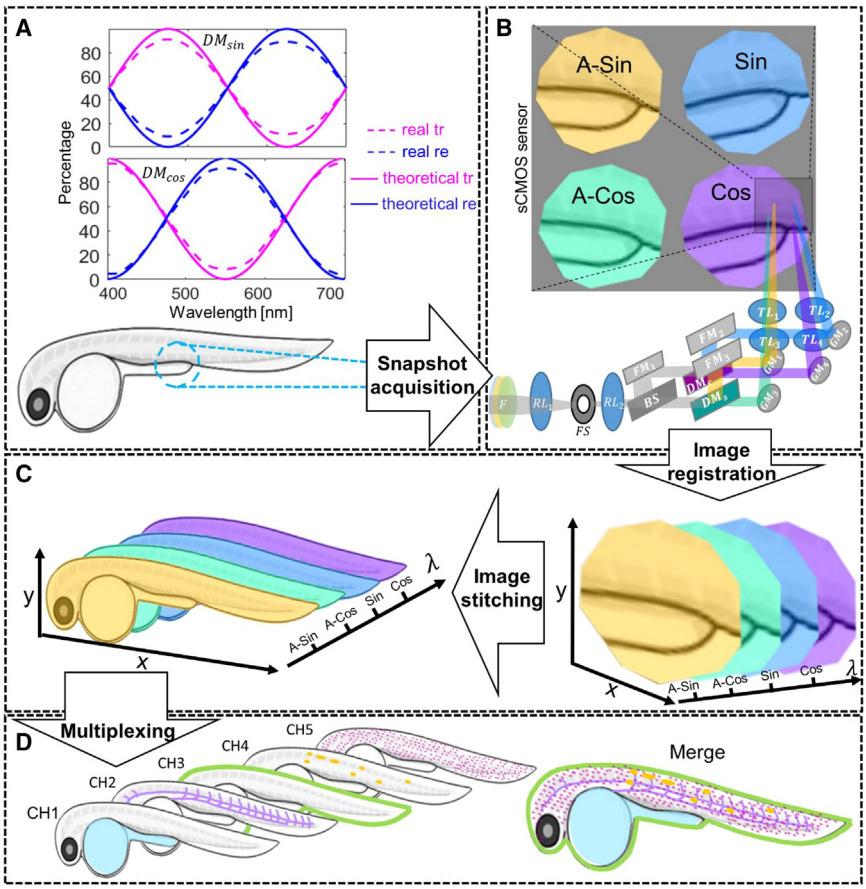

Figure 1. SHy-Cam approach overview

(A) Theoretical (solid line) and real (dashed line) transmission (tr) and reflection (re) profiles of the two custom sinusoidal dichroic mirrors (DM_{sin}, sine; DM_{cos}, cosine dichroic mirrors) in the range (400–700 nm). In this schematic representation, a fluorescently labeled zebrafish embryo provides signal input for the optical setup.

(B) Fluorescence emission is divided and encoded into four spectrally correlated channels using DM_{sin} and DM_{cos} before being projected onto a single sCMOS sensor. A zoomed-in view of the sensor illustrates this optical subdivision of the sensor (F, filter set; RL_{1-2}, relay lenses; FS, field stop; BS, 50/50 beamsplitter; FM_{1-3}, folding mirrors; DM_s, sine dichroic mirror; DM_c, cosine dichroic mirror; GM_{1-4}, gimbal mirrors; TL_{1-4}, tube lenses).

(C) Pre-processing (image registration and stitching) is performed on the four encoded channels to perform tiling of a large field of view.

(D) Multiplexing can be performed through any of multiple phasor approaches, separating the collected fluorescence into independent signals (CH1–CH5) and assembling them in a final volumetric dataset (merge).

captures four spectrally correlated channels simultaneously on the four quadrants of a single sCMOS camera sensor with a single snapshot (Figure 1; STAR Methods). The single-camera architecture simplifies the design and reduces the cost compared with a multi-camera setup. SHy-Cam utilizes readily available optical and opto-mechanical components, combined with a few custom-made 3D printed parts, which provides the advantage of easy replications and necessary modifications for new microscope adaptations. SHy-Cam is cost effective, as it does not require multiple specialized detection filters, filter changers, or complex dispersing and spatial mapping optics found in other approaches such as IMS; the cost of the complete list of parts and 3D printing models is approximately $6,000 (supplemental information).

SHy-Cam imaging validation tests

To validate the real-world performance of SHy-Cam, we integrated it into a custom SPIM[23,24] designed to offer optical sectioning and high-speed imaging capability. Its multiple single-photon laser lines permit simultaneous excitation of multiple fluorophores in the visible range (400–700 nm). Our first implementation with a simple 5M pixel sCMOS camera (PCO) offered a total magnification of 44×, including the magnification introduced by SHy-Cam itself, and an x-y field of view (FoV) in object space of 120 μm diagonally (Figures S1E–S1H; STAR Methods), requiring tiled acquisition for imaging larger specimens. The total magnification can be changed by using different objective lenses, relay lenses, or tube lenses (supplemental information) depending on the application.

As a first test of SHy-Cam, we imaged a set of different mixtures of two commonly used fluorescent dyes, Rhodamine B and Rhodamine 6G (Sigma-Aldrich) (Figure 2A); the emission spectrum of each mixture is mapped to a cluster on the 2D phasor plane showing reliable and distinct cluster locations for the dye mixtures with different mixing ratios (Figures 2B and 2C). SHy-CAM could distinguish small spectral changes of only 1.2% in relative concentrations, easily separating mixtures of ratio 1:12 from those of 1:14, for example (Figures 2C and 2D). The mixtures are visualized using Spectrally Encoded Enhanced Representations (SEER)-encoded colormap[25] with different colors representing the emission spectra of different relative concentrations (Figure 2D).

We tested fluorescent signal multiplexing using geometric segmentation on the 2D SP calculated from SHy-Cam images. Immobilized fluorescent beads (Bangs Laboratories, Sigma-Aldrich) with six distinct but highly overlapping spectra (Figure 2E) were imaged with SHy-Cam (Figure 2G). Pixels from the four channels were transformed into the phasor plane (STAR Methods), creating a look-up table linking pixels and corresponding phasor coefficients. These phasor coefficients were represented as a 2D histogram in the 2D phasor plane. Beads with the same spectral emission correspond to a single cluster on the 2D phasor plane (Figure 2F). Six clusters were selected with six circular regions of interests (ROIs) on the phasor plane (Figure 2F). The corresponding pixels were respectively pseudo-colored, permitting the unambiguous visualization of beads within the imaging volume (Figure 2G).

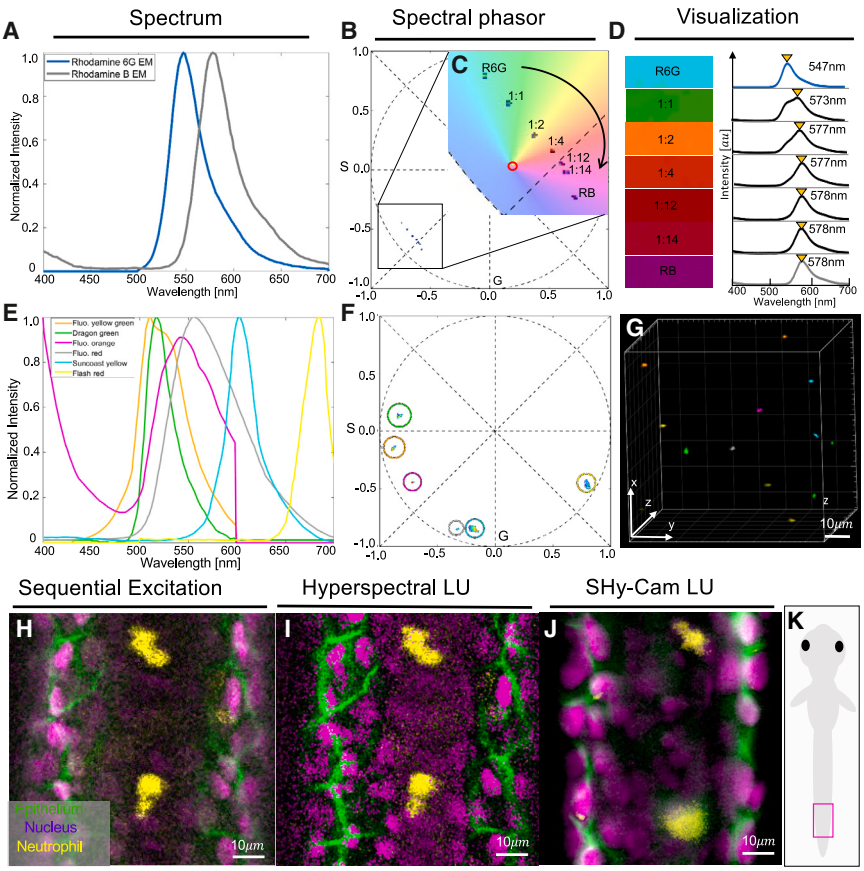

Figure 2. SHy-Cam spectral unmixing on standard and fixed samples

(A) Normalized emission spectra of Rhodamine 6G and Rhodamine B in water.

(B) Phasor plot demonstrating distinct clusters of pure Rhodamine 6G (R6G) and Rhodamine B (RB) and of five solution mixtures with different relative concentrations (R6G:RB).

(C) Zoomed-in view of phasor plot clusters in (B) visualized using the SEER phasor map encoding (red circle indicates the SEER map center for the morphed angle rendering of the spectral information).

(D) SEER pseudo-color bars representing each phasor cluster, with a continuous color map (bottom panel) showing the distinction of relative concentrations of the solutions. The emission profiles (400–700 nm) and peak emission wavelengths of each mixture are shown to the right of the corresponding pseudo-color bars; as RB relative concentration increases, the peak and shape of emission profile resembles pure RB.

(E) Fluorescence emission profiles of six different fluorescent beads.

(F) Spectral phasor calculated from the SHy-Cam image of a suspension of the beads mixture. Each cluster on the phasor plane represents beads from the same batch that present very similar fluorescence emission profiles (E). Six circular ROIs applied to the distinct phasor clusters are back mapped from phasor plane to a 3D image plane, highlighting the corresponding image pixels with the same ROI color coding to achieve unmixing.

(G) The unmixed image stack of the suspension. Beads were color coded with the same pseudo-colors of the corresponding circular ROIs on the phasor plane.

(H–J) Images of a triple-labeled zebrafish embryo collected with conventional and SHy-Cam microscopy. Green: membrane Tg(krt4:GFP), yellow: neutrophil Tg(lyz:TagRFP), purple: ubiquitous cell nucleus ubi:H2B-iRFP670. (H) Image acquired with Zeiss LSM 880 with sequential laser excitation for each fluorescent label, rendered as a maximum intensity projection (MIP) of a coronal plane of a 4 dpf fixed zebrafish embryo (inset, K). (I) The same region acquired with Zeiss LSM 880 using three-laser simultaneous excitation in 32-channel hyperspectral mode, rendered using linear unmixing (LU) for fluorescence separaton. (J) Spectral LU result from SHy-Cam image acquired from the same embryo, reasonably close to the confocal microscope images in (H) and (I). Scale bar for (H), (I), and (J): 10μm.

Multiplexing using 2D phasor plane segmentation is an intuitive and fast analysis method for spectrally overlapping but spatially sparse fluorescence. However, a clean and unambiguous signal separation can be challenging when fluorescent signals are spectrally and spatially overlapping. SHy-Cam added two reflected channels allow ratiometric analysis using spectral LU.[21,22] We tested SHy-Cam in multiplexing spatially and spectrally overlapping fluorescence of a fixed 3-color zebrafish embryo (STAR Methods) and compared the imaging results with data acquired on a reference system, a laser scanning confocal microscope (LSM-880, Carl Zeiss) equipped with a 32-channel spectral detector (STAR Methods). A similar coronal plane of the fixed sample was acquired on both LSM and Shy-CAM instruments (Figures 2H–2J). We acquired a "ground-truth" image on the confocal by sequentially exciting the fluorescent proteins in the sample, capturing three separate fluorescence emission datasets (Figure 2H). We then acquired a confocal 32-channel hyperspectral dataset by simultaneously exciting with the three lasers, followed by spectral LU to separate fluorescence signals (Figure 2I). Following this, we remounted the same fixed embryo for imaging on the SHy-Cam-SPIM using simultaneous excitation of three laser lines, similar to the LSM images, and used the same spectral LU analysis (STAR Methods; Figure 2J). The SHy-Cam unmixed results resemble closely the "ground truth" but were collected 4-fold faster than LSM in spectral imaging modality (Figure 2I) and 12-fold faster than sequential LSM acquisition (Figure 2H). The dataset reported in Figure 2J was acquired with one single SHy-Cam snapshot of 200 ms exposure, compared with ~900 ms for the 32-channel LSM spectral dataset (Figure 2I) and ~2,700 ms for the 3 sequential frames reported in Figure 2H.

SHy-Cam worked well for *in vivo* multiplexed volumetric imaging of transgenic zebrafish embryos with up to 5 colors. Figure 3 presents the results obtained from a 4 day post-fertilization (dpf) transgenic zebrafish embryo, separating the signals arising from 4 spatially and spectrally overlapping fluorescent proteins from one another and from the tissue-generated autofluorescence using spectral LU. The number of signals being unmixed is larger than the number of imaging channels on the sCMOS camera, making the LU appear to be an underdetermined system;

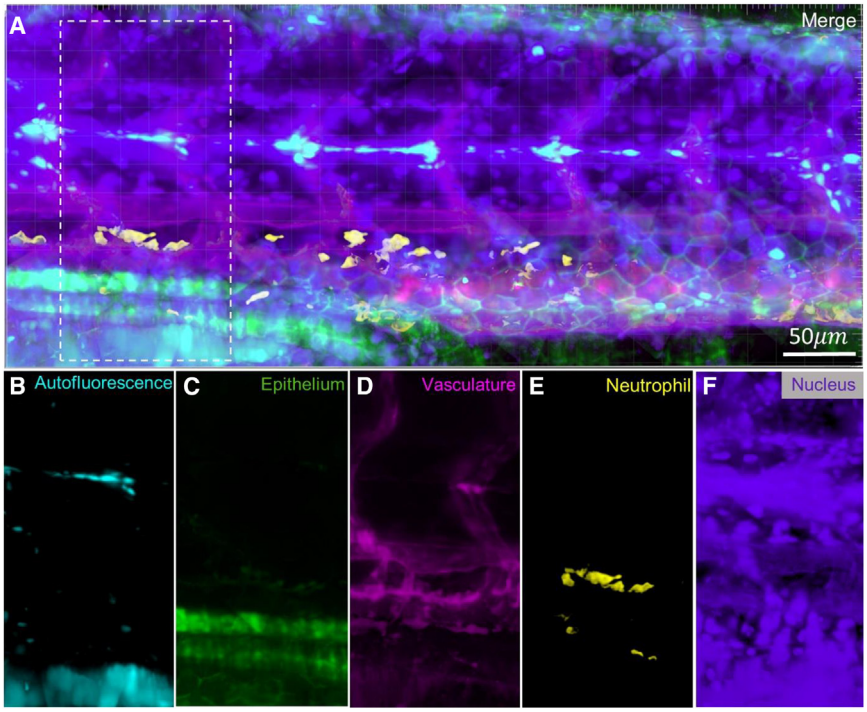

Figure 3. SHy-Cam-SPIM tiled volumetric *in vivo* imaging

(A) MIP image acquired from the trunk area of a 4 dpf transgenic zebrafish embryo; five labels were unmixed by LU from SHy-Cam image data (autofluorescence and four fluorescent proteins). The volumetric image consists of 21 tiles, each with 62 optical sections, covering a field of view of 602 × 256 × 120 μm. Scale bar for (A): 50μm.

(B–F) The individual unmixed fluorescence signals displayed for the subregion (dashed box) in (A): (B) cyan: autofluorescence, (C) green: membrane Tg(krt4:GFP), (D) magenta: vasculature Tg(kdrl:mCherry), (E) yellow: neutrophil Tg(lyz:TagRFP), and (F) purple: ubiquitous cell nucleus ubi:H2B-iRFP670.

however, the unmixing results reveal clean separation, even when the results are presented at high contrast (Figures 3B–3F) with minimal crosstalk as quantified in Figure S2. This result shows SHy-Cam's ability to capture sufficient fluorescence spectral information in challenging imaging conditions. The acquisition was conducted by simultaneous excitation of by three laser lines, with their powers adjusted to yield roughly similar emission intensity levels across the five labels in single exposures of 200 ms. Even including the inevitable time delays required for moving the specimen for tiling and for z stacking, the volumetric image of the embryo trunk area (Figure 3A; Video S1) was acquired in under 4 min.

SHy-Cam's rapid *in vivo* imaging capability is well suited to two distinct imaging challenges in live zebrafish embryos: cell migration and the beating heart. Cell migration was imaged at a high spatiotemporal resolution over a large FoV to follow the migration of neutrophils toward a zebrafish tail-clipping wound (Figures 4A–4D; Video S2). For each time point, a mosaic of volumes was collected with the co-excitation of 3 laser lines; the tiles were stitched together and analyzed with spectral LU. The imaging rate of 2.7 volumetric tiles per minute offered sufficient temporal resolution to unambiguously track neutrophil migration. SHy-Cam's high detection efficiency for fluorescent signals combined with the advantages of light-sheet microscopy permitted continuous and prolonged time-lapse imaging with only 11% photo-bleaching (Figure 4J; Video S2). This permitted high-resolution imaging with no photo-toxicity to the embryo.

Imaging the beating heart is even more demanding. SHy-Cam was used to image the heart continuously at 20 frames per second for 10 s (Video S3; Figures 4F–4I). This high-speed acquisition was sufficient to track the fast-moving neutrophils (up to 200 μm/s) as they flowed across the atrial cavity. The excitation laser power was increased to minimize the camera exposure without inducing visible photo-damage in the sample. The rapid and continuous imagining resulted in only 4% photo-bleaching in the 10 s acquisition (Figure 4J). Because each frame captured all spectral information, there were no movement artifacts, providing striking multiplexing of fluorescent labels.

We performed high-speed imaging on a zebrafish embryo expressing a different combination of transgenic fluorescent proteins (Video S4) at 33 frames/s. The single-plane SPIM image captured a cross-sectional recording of the movement of the nuclei in the cells of the atrial wall while the heart is beating at around 180 beats/min. These results highlight SHy-Cam's ability to perform challenging high-speed multiplexed fluorescence imaging.

DISCUSSION

Our results demonstrate that SHy-Cam offers an efficient and rapid multiplexed imaging of fluorescent signals. The speed and photon efficiency are significant advantages, especially in the applications involving *in vivo* timelapse and volumetric imaging, to minimize acquisition time and photo-bleaching in the sample. The SP encoding captures the differences between similar fluorescent signatures but removes the redundancy of the traditional uniform hyperspectral sampling strategies, improving not only photon efficiency but also processing and data storage needs. SHy-Cam's single-snapshot acquisition achieves more than 10-fold faster imaging speed compared with the existing filter-based SP approach,[18,19] benefiting imaging applications with rapid dynamics or development of biological systems. Compared with sequential acquisition, SHy-Cam eliminates the need for channel realignment, reducing spectral distortions and motion blur (Figure S3). In addition, SHy-Cam's added spectral information by recycling the reflected photons[20] enables ratiometric fluorescence multiplexing using spectral LU.[21,22]

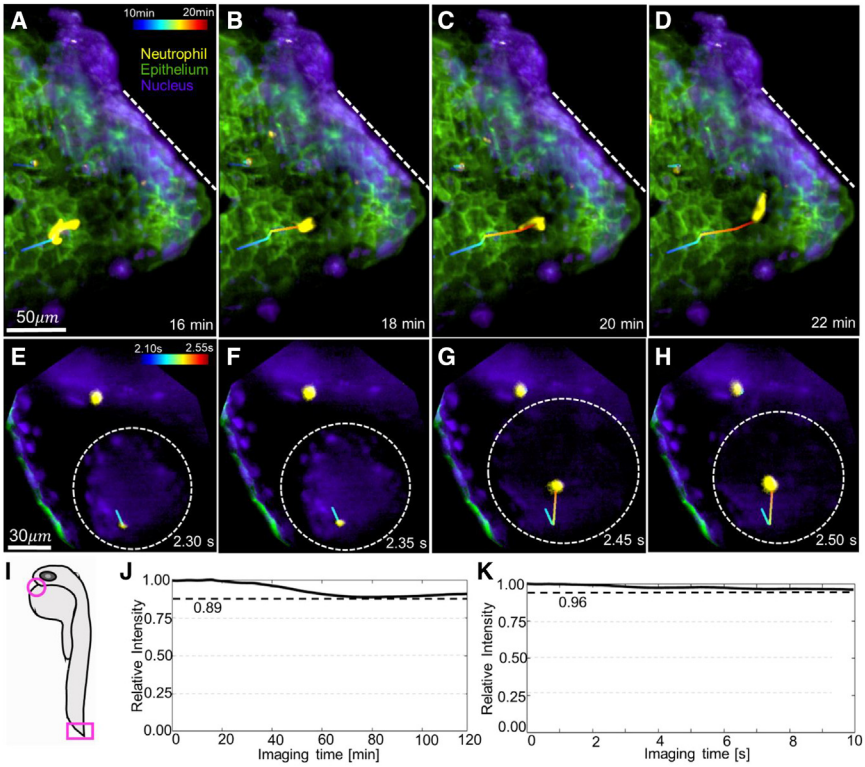

Figure 4. SHy-Cam-SPIM dynamic *in vivo* imaging

(A–D) Zebrafish tail-clip wound healing (dashed line) acquired as a 2 h tiled volumetric timelapse. The transgenic embryos are labeled in their cell membranes (green; Tg(krt4:GFP)), nuclei (purple; ubi:H2B-iRFP670), and neutrophils (yellow; Tg (lyz:TagRFP)). Neutrophil migration toward the wound can be observed at high resolution in 3D in the context of tissues and tracked over time. Scale bar for (A–D): 50μm.

(E–H) The same embryo's beating heart (dashed circles) is captured continuously at 20 frames/s for 10 s covering an area of 17.1×10^3 μm^2. Neutrophils flowing through the cardiac area can be tracked (jet dragon tail). Scale bar for (E–H): 30μm.

(I) Zebrafish embryo representing the imaging positions of (A)–(D) (square) and (E)–(H) (circle). The volumetric images are each composed of 6 tiles, each of 21 optical sections (Video S2), covering a field of view of 300 × 250 × 42 μm. The frames displayed here are taken from a timelapse recording of 60 timepoints acquired quasi-continuously.

(J and K) Photo-bleaching is estimated as relative intensity of the emission signal from all channels during the 2 h tail-clip wound healing timelapse imaging and during the 10 s heart beating timelapse.

We designed SHy-Cam focusing on the versatility, cost effectiveness, and accessibility. The versatile modular design was easily adapted to commercial microscopes and custom-built SPIMs, showing its potential for applications to any camera-based systems. While the SHy-Cam implementation in this work utilizes a single-camera architecture to remove the necessity of utilizing and synchronizing multiple expensive sCMOS cameras, it could easily be adapted to other implementations using two or four cameras. In addition, the design can be adapted to enable multifocal, line-scan, or point-scan confocal laser scanning microscopes using sets or arrays of silicon-based detectors or photo-multiplier tubes (PMTs).

The SHy-Cam data rendering on the 2D phasor plot offers intuitive and fast display and interactive analysis of multiplexing data.[17,25] The same data can be analyzed with spectral LU, enabling ratiometric fluorescence multiplexing even in the presence of significant spatial and spectral overlap between multiple fluorophores or between the labels and high background fluorescence. SHy-Cam is poised to be a solution for high-speed and -throughput imaging and multiplexing applications where improved detection at low signal and at low SNR would considerably shorten experimental pipelines.

Besides *in vivo* fluorescence imaging applications, other applications such as multi-color high-content cellular analyses are poised to benefit from SHy-Cam's efficiency, streamlined spectral analysis, and visualization using the SP. Recent advancements in imaging flow cytometry (IFC)[26–33] have focused on overcoming the common trade-off between throughput, sensitivity, and spatial resolution of traditional IFC.[34] The same advantages of SHy-Cam demonstrated here for microscopy position it as a powerful means to improve other quantitative detection and multiplexing applications such as IFC.

SHy-Cam is poised as a solution for high-speed and -throughput fluorescent imaging applications where improved detection at low SNR and low signal conditions, combined with multiplexing, should considerably speed analyses and shorten experimental pipelines.

Limitations of study

A potential limitation of the single-camera SHy-Cam implementation here is the reduced FoV, resulting from the subdivision of the sensor into four quadrants. Here, we compensated for this by tiling our acquisition to achieve the same FoV as a non-subdivided sensor. Pilot implementations have shown that we can achieve the same advantages as the single SHy-Cam design presented here but over large FoVs by employing multiple sCMOS cameras or the growing set of large sCMOS sensors with many more pixels. Of course, for applications where spatial resolution is not demanding, a lower magnification relay lenses can offer a full FoV with improved SNR and excellent spectral sensitivity but at reduced spatial resolution.

The 50:50 beam splitter (Figure 1B), equally dividing the emission signal into two light paths for the simultaneous spectral encoding, might reduce the lowest light level performance of SHy-Cam, given the electronic noise of each pixel of the camera. For each channel, the numbers of photons reaching the detector are halved. The contribution of this reduction may be less than it first appears, as no detection filter passes 100% of the light in its band pass, and by its very nature, a band-pass filter rejects many photons that SHy-Cam would collect. SHy-Cam's redistribution

of light on the sensor, rather than rejection of the unwanted spectral ranges, provides a higher efficiency in the total number of photons detected, allowing higher spectral information collection and a faster single-snapshot acquisition. With the ongoing development of detectors with lower noise and with larger number of pixels (permitting pixel binning if needed), the low-light performance of SHy-Cam should meet or exceed that of other approaches.

STAR★METHODS

Detailed methods are provided in the online version of this paper and include the following:

- KEY RESOURCES TABLE
- RESOURCE AVAILABILITY
  - Lead contact
  - Materials availability
  - Data and code availability
- EXPERIMENTAL MODEL AND SUBJECT DETAILS
- METHOD DETAILS
  - Spectral compression with spectral phasor
  - Sinusoidal dichroic mirror
  - Optical design and setup
  - Opto-mechanics
  - Image acquisition
  - Image pre-processing
  - Image analysis
  - Photon-efficiency and -throughput estimation
  - Sample preparation
- QUANTIFICATION AND STATISTICAL ANALYSIS
  - SHy-Cam-SPIM dynamic in-*vivo* imaging photobleaching estimation
  - Signal crosstalk analysis of SHy-Cam spectral linear unmixing
  - SHy-Cam photon efficiency estimation

SUPPLEMENTAL INFORMATION

Supplemental information can be found online at https://doi.org/10.1016/j.crmeth.2023.100441.

ACKNOWLEDGMENTS

This project was supported by US Department of Defense (PR150666), Chan Zuckerberg Initiative (CZI), and University of Southern California.

AUTHOR CONTRIBUTIONS

P.W. designed and built the SHy-Cam system and conducted experiments and research study. M.K. raised zebrafish lines and set up cross for embryos that were used as *in vivo* imaging samples. T.V.T built the SPIM. K.K.-D. provided advice on adapting the SHy-Cam prototype onto SPIM. F.C. and S.E.F. conceived the original idea and provided systematic advice in this project. All authors discussed the conclusions and commented on the manuscript.

DECLARATION OF INTERESTS

The University of Southern California has filed a provisional patent application covering this method listing P.W., S.E.F., and F.C. as inventors.

Received: April 21, 2022
Revised: November 16, 2022
Accepted: March 9, 2023
Published: March 31, 2023

REFERENCES

1. Jahr, W., Schmid, B., Schmied, C., Fahrbach, F.O., and Huisken, J. (2015). Hyperspectral light sheet microscopy. Nat. Commun. *6*, 7990. https://doi.org/10.1038/ncomms8990.
2. Mahou, P., Zimmerley, M., Loulier, K., Matho, K.S., Labroille, G., Morin, X., Supatto, W., Livet, J., Débarre, D., and Beaurepaire, E. (2012). Multicolor two-photon tissue imaging by wavelength mixing. Nat. Methods *9*, 815–818. https://doi.org/10.1038/nmeth.2098.
3. Valm, A.M., Cohen, S., Legant, W.R., Melunis, J., Hershberg, U., Wait, E., Cohen, A.R., Davidson, M.W., Betzig, E., and Lippincott-Schwartz, J. (2017). Applying systems-level spectral imaging and analysis to reveal the organelle interactome. Nature *546*, 162–167. https://doi.org/10.1038/nature22369.
4. Levenson, R.M., and Mansfield, J.R. (2006). Multispectral imaging in biology and medicine: slices of life. Cytometry A. *69*, 748–758. https://doi.org/10.1002/cyto.a.20319.
5. Lavagnino, Z., Dwight, J., Ustione, A., Nguyen, T.U., Tkaczyk, T.S., and Piston, D.W. (2016). Snapshot hyperspectral light-sheet imaging of signal transduction in live pancreatic islets. Biophys. J. *111*, 409–417. https://doi.org/10.1016/j.bpj.2016.06.014.
6. Huisken, J., Swoger, J., del Bene, F., Wittbrodt, J., and Stelzer, E.H.K. (2004). Optical sectioning deep inside live embryos by selective plane illumination microscopy. Science *305*, 1007–1009. https://doi.org/10.1126/science.1100035.
7. Huisken, J., and Stainier, D.Y.R. (2009). Selective plane illumination microscopy techniques in developmental biology. Development *136*, 1963–1975. https://doi.org/10.1242/dev.022426.
8. Power, R.M., and Huisken, J. (2017). A guide to light-sheet fluorescence microscopy for multiscale imaging. Nat. Methods *14*, 360–373. https://doi.org/10.1038/nmeth.4224.
9. Keomanee-Dizon, K., Fraser, S.E., and Truong, T.V. (2020). A versatile, multi-laser twin-microscope system for light-sheet imaging. Rev. Sci. Instrum. *91*, 053703. https://doi.org/10.1063/1.5144487.
10. Chhetri, R.K., Amat, F., Wan, Y., Höckendorf, B., Lemon, W.C., and Keller, P.J. (2015). Whole-animal functional and developmental imaging with isotropic spatial resolution. Nat. Methods *12*, 1171–1178. https://doi.org/10.1038/nmeth.3632.
11. Mickoleit, M., Schmid, B., Weber, M., Fahrbach, F.O., Hombach, S., Reischauer, S., and Huisken, J. (2014). High-resolution reconstruction of the beating zebrafish heart. Nat. Methods *11*, 919–922. https://doi.org/10.1038/nmeth.3037.
12. Mahou, P., Vermot, J., Beaurepaire, E., and Supatto, W. (2014). Multicolor two-photon light-sheet microscopy. Nat. Methods *11*, 600–601. https://doi.org/10.1038/nmeth.2963.
13. Bedard, N., Hagen, N., Gao, L., and Tkaczyk, T.S. (2012). Image mapping spectrometry: calibration and characterization. Opt. Eng. *51*, 111711. https://doi.org/10.1117/1.oe.51.11.111711.
14. Fereidouni, F., Bader, A.N., and Gerritsen, H.C. (2012). Spectral phasor analysis allows rapid and reliable unmixing of fluorescence microscopy spectral images. Opt Express *20*, 12729–12741. https://doi.org/10.1364/oe.20.012729.
15. Andrews, L.M., Jones, M.R., Digman, M.A., and Gratton, E. (2013). Spectral phasor analysis of Pyronin Y labeled RNA microenvironments in living cells. Biomed. Opt Express *4*, 171–177. https://doi.org/10.1364/boe.4.000171.
16. Cutrale, F., Salih, A., and Gratton, E. (2013). Spectral phasor approach for fingerprinting of photo-activatable fluorescent proteins Dronpa, Kaede

and KikGR. Methods Appl. Fluoresc. *1*, 35001. https://doi.org/10.1088/2050-6120/1/3/035001.

17. Cutrale, F., Trivedi, V., Trinh, L.A., Chiu, C.-L., Choi, J.M., Artiga, M.S., and Fraser, S.E. (2017). Hyperspectral phasor analysis enables multiplexed 5D in vivo imaging. Nat. Methods *14*, 149–152. https://doi.org/10.1038/nmeth.4134.
18. Dvornikov, A., and Gratton, E. (2018). Hyperspectral imaging in highly scattering media by the spectral phasor approach using two filters. Biomed. Opt Express *9*, 3503–3511. https://doi.org/10.1364/boe.9.003503.
19. Hedde, P.N., Cinco, R., Malacrida, L., Kamaid, A., and Gratton, E. (2021). Phasor-based hyperspectral snapshot microscopy allows fast imaging of live, three-dimensional tissues for biomedical applications. Commun. Biol. *4*, 721. https://doi.org/10.1038/s42003-021-02266-z.
20. Zhang, Y., Schroeder, L.K., Lessard, M.D., Kidd, P., Chung, J., Song, Y., Benedetti, L., Li, Y., Ries, J., Grimm, J.B., et al. (2020). Nanoscale subcellular architecture revealed by multicolor three-dimensional salvaged fluorescence imaging. Nat. Methods *17*, 225–231. https://doi.org/10.1038/s41592-019-0676-4.
21. Dickinson, M.E., Bearman, G., Tille, S., Lansford, R., and Fraser, S.E. (2001). Multi-spectral imaging and linear unmixing add a whole new dimension to laser scanning fluorescence microscopy. Biotechniques *31*, 1272, 1274-6, 1278. https://doi.org/10.2144/01316bt01.
22. Zimmermann, T. (2005). Spectral imaging and linear unmixing in light microscopy. Adv. Biochem. Eng. Biotechnol. *95*, 245–265. https://doi.org/10.1007/b102216.
23. Truong, T.V., Supatto, W., Koos, D.S., Choi, J.M., and Fraser, S.E. (2011). Deep and fast live imaging with two-photon scanned light-sheet microscopy. Nat. Methods *8*, 757–760. https://doi.org/10.1038/nmeth.1652.
24. Trivedi, V., Truong, T.V., Trinh, L.A., Holland, D.B., Liebling, M., and Fraser, S.E. (2015). Dynamic structure and protein expression of the live embryonic heart captured by 2-photon light sheet microscopy and retrospective registration. Biomed. Opt Express *6*, 2056–2066. https://doi.org/10.1364/boe.6.002056.
25. Shi, W., Koo, D.E.S., Kitano, M., Chiang, H.J., Trinh, L.A., Turcatel, G., Steventon, B., Arnesano, C., Warburton, D., Fraser, S.E., and Cutrale, F. (2020). Pre-processing visualization of hyperspectral fluorescent data with spectrally encoded enhanced representations. Nat. Commun. *11*, 726. https://doi.org/10.1038/s41467-020-14486-8.
26. Sancho, D., Joffre, O.P., Keller, A.M., Rogers, N.C., Martínez, D., Hernanz-Falcón, P., Rosewell, I., and Reis e Sousa, C. (2009). Identification of a dendritic cell receptor that couples sensing of necrosis to immunity. Nature *458*, 899–903. https://doi.org/10.1038/nature07750.
27. Tse, H.T.K., Gossett, D.R., Moon, Y.S., Masaeli, M., Sohsman, M., Ying, Y., Mislick, K., Adams, R.P., Rao, J., and Di Carlo, D. (2013). Quantitative diagnosis of malignant pleural effusions by single-cell mechanophenotyping. Sci. Transl. Med. *5*, 212ra163. https://doi.org/10.1126/scitranslmed.3006559.
28. Ralston, K.S., Solga, M.D., MacKey-Lawrence, N.M., Somlata, Bhattacharya, A., and Petri, W.A. (2014). Trogocytosis by Entamoeba histolytica contributes to cell killing and tissue invasion. Nature *508*, 526–530. https://doi.org/10.1038/nature13242.
29. Maryanovich, M., Zaltsman, Y., Ruggiero, A., Goldman, A., Shachnai, L., Zaidman, S.L., Porat, Z., Golan, K., Lapidot, T., and Gross, A. (2015). An MTCH2 pathway repressing mitochondria metabolism regulates haematopoietic stem cell fate. Nat. Commun. *6*, 7901. https://doi.org/10.1038/ncomms8901.
30. Basiji, D., and O'Gorman, M.R.G. (2015). Imaging flow cytometry. J. Immunol. Methods *423*, 1–2. https://doi.org/10.1016/j.jim.2015.07.002.
31. Otto, O., Rosendahl, P., Mietke, A., Golfier, S., Herold, C., Klaue, D., Girardo, S., Pagliara, S., Ekpenyong, A., Jacobi, A., et al. (2015). Real-time deformability cytometry: on-the-fly cell mechanical phenotyping. Nat. Methods *12*, 199–202, 4 p following 202. https://doi.org/10.1038/nmeth.3281.
32. Sykes, D.B., Kfoury, Y.S., Mercier, F.E., Wawer, M.J., Law, J.M., Haynes, M.K., Lewis, T.A., Schajnovitz, A., Jain, E., Lee, D., et al. (2016). Inhibition of dihydroorotate dehydrogenase overcomes differentiation blockade in acute myeloid leukemia. Cell *167*, 171–186.e15. https://doi.org/10.1016/j.cell.2016.08.057.
33. Vorobjev, I.A., and Barteneva, N.S. (2016). Imaging Flow Cytometry Methods and Protocols (Humana Press).
34. Mikami, H., Kawaguchi, M., Huang, C.J., Matsumura, H., Sugimura, T., Huang, K., Lei, C., Ueno, S., Miura, T., Ito, T., et al. (2020). Virtual-freezing fluorescence imaging flow cytometry. Nat. Commun. *11*, 1162. https://doi.org/10.1038/s41467-020-14929-2.
35. Lee, R.T.H., Asharani, P.V., and Carney, T.J. (2014). Basal keratinocytes contribute to all strata of the adult zebrafish epidermis. PLoS One *9*, e84858. https://doi.org/10.1371/journal.pone.0084858.
36. Lam, P.-Y., Yoo, S.K., Green, J.M., and Huttenlocher, A. (2012). The SH2-domain-containing inositol 5-phosphatase (SHIP) limits the motility of neutrophils and their recruitment to wounds in zebrafish. Journal of Cell Science *125*, 4973–4978. https://doi.org/10.1242/jcs.106625.
37. Proulx, K., Lu, A., and Sumanas, S. (2010). Cranial vasculature in zebrafish forms by angioblast cluster-derived angiogenesis. Dev. Biol. *348*, 34–46. https://doi.org/10.1016/j.ydbio.2010.08.036.
38. Schindelin, J., Arganda-Carreras, I., Frise, E., Kaynig, V., Longair, M., Pietzsch, T., Preibisch, S., Rueden, C., Saalfeld, S., Schmid, B., et al. (2012). Fiji: an open-source platform for biological-image analysis. Nat. Methods *9*, 676–682. https://doi.org/10.1038/nmeth.2019.
39. Edelstein, A.D., Tsuchida, M.A., Amodaj, N., Pinkard, H., Vale, R.D., and Stuurman, N. (2014). Advanced methods of microscope control using μManager software. J. Biol. Methods *1*, e10. https://doi.org/10.14440/jbm.2014.36.
40. Edelstein, A., Amodaj, N., Hoover, K., Vale, R., and Stuurman, N. (2010). Computer control of microscopes using manager. Curr. Protoc. Mol. Biol. *Chapter 14*, Unit14.20. https://doi.org/10.1002/0471142727.mb1420s92.
41. Trinh, L.A., Chong-Morrison, V., Gavriouchkina, D., Hochgreb-Hägele, T., Senanayake, U., Fraser, S.E., and Sauka-Spengler, T. (2017). Biotagging of specific cell populations in zebrafish reveals gene regulatory logic encoded in the nuclear transcriptome. Cell Rep. *19*, 425–440. https://doi.org/10.1016/j.celrep.2017.03.045.
42. White, R.M., Sessa, A., Burke, C., Bowman, T., LeBlanc, J., Ceol, C., Bourque, C., Dovey, M., Goessling, W., Burns, C.E., and Zon, L.I. (2008). Transparent adult zebrafish as a tool for in vivo transplantation analysis. Cell Stem Cell *2*, 183–189. https://doi.org/10.1016/j.stem.2007.11.002.
43. Parichy, D.M., Ransom, D.G., Paw, B., Zon, L.I., and Johnson, S.L. (2000). An orthologue of the kit-related gene fms is required for development of neural crest-derived xanthophores and a subpopulation of adult melanocytes in the zebrafish, Danio rerio. Development *127*, 3031–3044.
44. Huss, D., Benazeraf, B., Wallingford, A., Filla, M., Yang, J., Fraser, S.E., and Lansford, R. (2015). A transgenic quail model that enables dynamic imaging of amniote embryogenesis. Development *142*, 2850–2859. https://doi.org/10.1242/dev.121392.
45. Kwan, K.M., Fujimoto, E., Grabher, C., Mangum, B.D., Hardy, M.E., Campbell, D.S., Parant, J.M., Yost, H.J., Kanki, J.P., and Chien, C.B. (2007). The Tol2kit: a multisite gateway-based construction Kit for Tol2 transposon transgenesis constructs. Dev. Dyn. *236*, 3088–3099. https://doi.org/10.1002/dvdy.21343.
46. Kawakami, K., Takeda, H., Kawakami, N., Kobayashi, M., Matsuda, N., and Mishina, M. (2004). A transposon-mediated gene trap approach identifies developmentally regulated genes in zebrafish. Dev. Cell *7*, 133–144. https://doi.org/10.1016/j.devcel.2004.06.005.
47. Urasaki, A., Morvan, G., and Kawakami, K. (2006). Functional dissection of the Tol2 transposable element identified the minimal cis-sequence and a highly repetitive sequence in the subterminal region essential for

transposition. Genetics *174*, 639–649. https://doi.org/10.1534/genetics.106.060244.

48. Uren, A.G., Mikkers, H., Kool, J., Van Der Weyden, L., Lund, A.H., Wilson, C.H., Rance, R., Jonkers, J., Van Lohuizen, M., Berns, A., and Adams, D.J. (2009). A high-throughput splinkerette-pcr method for the isolation and sequencing of retroviral insertion sites. Nat. Protoc. *4*, 789–798. https://doi.org/10.1038/nprot.2009.64.

49. Trinh, L.A., Hochgreb, T., Graham, M., Wu, D., Ruf-Zamojski, F., Jayasena, C.S., Saxena, A., Hawk, R., Gonzalez-Serricchio, A., Dixson, A., et al. (2011). A versatile gene trap to visualize and interrogate the function of the vertebrate proteome. Genes Dev. *25*, 2306–2320. https://doi.org/10.1101/gad.174037.111.

50. Bogovic, J.A., Hanslovsky, P., Wong, A., and Saalfeld, S. (2016). Robust registration of calcium images by learned contrast synthesis. In Proceedings - International Symposium on Biomedical Imaging. https://doi.org/10.1109/ISBI.2016.7493463.

51. Goshtasby, A. (1988). Image registration by local approximation methods. Image Vis Comput. *6*, 255–261. https://doi.org/10.1016/0262-8856(88)90016-9.

52. Goldberg, I.G., Allan, C., Burel, J.M., Creager, D., Falconi, A., Hochheiser, H., Johnston, J., Mellen, J., Sorger, P.K., and Swedlow, J.R. (2005). The Open Microscopy Environment (OME) Data Model and XML file: open tools for informatics and quantitative analysis in biological imaging. Genome Biol. *6*, R47. https://doi.org/10.1186/gb-2005-6-5-r47.

53. Hedde, N., Cinco, R., Malacrida, L., Kamaid, A., and Gratton, E. (2020). Ultrafast phasor-based hyperspectral snapshot microscopy for biomedical imaging. Preprint at bioRxiv. https://doi.org/10.1101/2020.10.14.339416.

STAR★METHODS

KEY RESOURCES TABLE

REAGENT or RESOURCE	SOURCE	IDENTIFIER
Chemicals, peptides, and recombinant proteins		
1-μm, 1% solid fluorescent bead samples red	Sigma-Aldrich	L2778
1-μm, 1% solid fluorescent bead samples yellow-green	Sigma-Aldrich	L1030
1-μm, 1% solid fluorescent bead samples orange	Sigma-Aldrich	L9654
1-μm, 1% solid fluorescent bead samples Dragon Green	Bangs Laboratories, Inc.	N/A
1-μm, 1% solid fluorescent bead samples Flash Red	Bangs Laboratories, Inc.	N/A
1-μm, 1% solid fluorescent bead samples Suncoast Yellow	Bangs Laboratories, Inc.	N/A
Deposited data		
SHy-Cam raw and spectral linear unmixed data	This paper	Mendeley Data: https://doi.org/10.17632/6y7hjyb8px.1
Experimental models: Organisms/strains		
Zebrafish: Tg(krt4:GFP)	Lee et al.[35]	ZFIN: ZDB-FIG-140403-34
Zebrafish: Tg(lyz:TagRFP)	Lam et al.[36]	ZFIN: ZDB-TGCONSTRCT-121008-1
Zebrafish: ubi:H2B-iRFP670	This work	N/A
Zebrafish: Tg(kdrl:mCherry)	Proulx et al.[37]	ZFIN: ZDB-ALT-110131-57
Software and algorithms		
FIJI	Schindelin et al.[38]	https://imagej.net/software/fiji/
Matlab	Mathworks	https://mathworks.com
Imaris Stitcher	Oxford Instruments	https://imaris.oxinst.com/products/imaris-stitcher
Micro-Manager	Edelstein et al.[39,40]	https://doi.org/10.14440/jbm.2014.36, https://doi.org/10.1002/0471142727.mb1420s92
SHy-Cam image pre-processing and spectral linear unmixing script	This paper	https://doi.org/10.5281/zenodo.7672758

RESOURCE AVAILABILITY

Lead contact

Further information and should be directed to the lead contact, Francesco Cutrale (cutrale@usc.edu).

Materials availability

This study did not generate new unique reagents.

Data and code availability

- SHy-Cam zebrafish in-*vivo* imaging datasets have been deposited at Mendeley Database and are publicly available as of the date of publication. DOI is listed in the key resources table.
- The original MATLAB code for SHy-Cam image pre-processing and spectra linear unmixing has been deposited on Github at https://github.com/PaulWZZtoLA/Singleshot-Hyperspectral-Phasor-Camera-SHyCam. (https://doi.org/10.5281/zenodo.7672758). HySP software download and instruction can be found at http://bioimaging.usc.edu/software.html#HySP.
- Any additional information required to reanalyze the data reported in this paper is available from the lead contact upon request.

EXPERIMENTAL MODEL AND SUBJECT DETAILS

Zebrafish lines were raised and maintained following standard literature practice and in accordance with the Guide for the Care and Use of Laboratory Animals provided by the University of Southern California. Fish samples were part of a protocol approved by the

IACUC (permit number: 12007 USC). krt4:lyn-egfp and krtt1c19e:lyn-tdtomato transgenic lines[35] were kind gifts from Thomas J. Carney (A*STAR, Singapore). kdrl:mCherry transgenic line[37] was a kind gift from Ching-Ling Lien (Children's Hospital Los Angeles). TgBAC(sox10:BirA-mCherry)ox104a line was reported previously.[41] *mpv17*$^{a9/a9}$*;mitfa*$^{w2/w2}$ (*casper*) line[42] was purchased from Zebrafish International Resource Center (ZIRC) and *csf1r*$^{j4e1/j4e1}$ (*panther*) line[43] was a kind gift from David Parichy (Univ. Virginia). We crossed *casper* with *panther* to produce triple heterozygote *mpv17*$^{a9/+}$*;mitfa*$^{w2/+}$*;csf1r*$^{j4e1/+}$ F1 generation fish, which were subsequently incrossed to produce F2 generation with 27 combinations of mutational state of these genes. Since *csf1r*^{j4e1} phenotype was not clear in F2 adult with *casper* phenotype, we outcrossed these fish with *panther* fish to determine the zygosity of *csf1r*^{j4e1} mutation based on the frequency of larva with xanthophores (heterozygote and homozygote produced 50%- and 0%-fraction of xanthophore-positive larva, respectively) by fluorescent microscopy. The *casper;csf1r*$^{j4e1/j4e1}$ line is viable and reproducible; we outcrossed either *casper;csf1r*$^{j4e1/j4e1}$ line or *casper;csf1r*$^{j4e1/+}$ line with other fluorescent transgenic lines over several generations to obtain fish harboring multiple transgenes on *casper* background either in the presence or absence of xanthophores.

The coding sequences for human Histone 2b region (H2B) and fluorescent protein iRFP670 were amplified from the vector for Tg(PGK1:H2B-chFP)[44] using primers #1 and #2, and piRFP670-N1 (Addgene # 45457) using primers #3 and #4, respectively. The PCR products were fused to generate H2B-iRFP670 fusion fragment and cloned into pDONR221 (Thermo Fisher Scientific). Subsequent MultiSite Gateway reaction was performed using Tol2kit vectors according to developer's manuals.[45] pENTR5'ubi (Addgene #27320), pDONR221-H2B-iRFP670, and pDONR P2R-P3-WPRE[25] were assembled into pDestTol2pA2 (Tol2kit #394).[46,47] The resultant pDestTol2-ubi:H2B-iRFP670 was co-injected with tol2 mRNA into one-cell-stage casper zebrafish embryos. Injected F0s were raised and screened for founders. Positive F1s grown to reproductive age were subjected to Splinklette PCR analysis[48,49] to determine genomic integration sites. Embryos that had specific expressions of transgenic fluorescent proteins were collected and raised in a low-salt embryo medium per established procedures until the appropriate time (*4dpf*) for imaging. Sex of zebrafish samples cannot be properly identified at these early stage of development.

METHOD DETAILS

Spectral compression with spectral phasor

Spectral phasor is an established Fourier transform-based analysis method of hyperspectral data that compresses high dimensional spectral vectors into their normalized first harmonic Fourier coefficients[14–17] represented by Equations 1 and 2. The linear additive property of fluorescence emission and their wide spectral profile of common fluorescence make it possible to recover substantial amount of spectral information with the 'base frequency' and DC components of hyperspectral data (supplemental information).

$$G = \frac{\sum_{n=0}^{N-1} I(\lambda_n) \cdot \cos\left(\frac{2\pi}{N}\lambda\right) * \Delta\lambda}{\sum_{n=0}^{N-1} I(\lambda_n) * \Delta\lambda} \quad \text{(Equation 1)}$$

$$S = \frac{\sum_{n=0}^{N-1} I(\lambda_n) \cdot \cos\left(\frac{2\pi}{N}\lambda\right) * \Delta\lambda}{\sum_{n=0}^{N-1} I(\lambda_n) * \Delta\lambda} \quad \text{(Equation 2)}$$

G and *S* are the real and imaginary coefficients, called phasor coefficients. λ_n represents the wavelength of the n-*th* spectral channel out of a N-channel spectral vector. $I(\lambda_n)$ denotes the intensity value of the n-*th* channel. $\Delta\lambda$ is the wavelength bandwidth of a single channel. The denominators in Equation 1 represent the integral of the intensity values across all N channels and are the normalization factors that eliminate the influence of different intensity levels, which also incorporates the DC component of the spectral vector. Phasor coefficients are visually presented as a 2-D histogram called phasor plane (Figures 2B and 2F). Each (*G,S*) pair corresponds to a unique spectral vector in the original hyperspectral image plane.

SHy-Cam performs spectral phasor compression optically during acquisition and directly get the unnormalized *G,S* phasor coefficients via transmitting the emission through two custom sinusoidal dichroic mirrors (Figures 1A and 1B), similar to filter-based spectral phasor approach.[18,19] 'SIN' and 'COS' channels shown in (Figure 1B) are the transmitted channels that can be used to estimate phasor coefficients with some simple calculation. 'ASIN' and 'ACOS' channels are the reflected channels. Phasor coefficients calculation from SHy-Cam is represented with Equations 3, 4). As transmitted and reflected emission are collected at the same time, the normalization factor, i.e. the intensity value, is readily available by summing 'SIN' with 'ASIN' or 'COS' with 'ACOS' (5).

$$G = \frac{C_{ideal}}{I} \quad \text{(Equation 3)}$$

$$S = \frac{S_{ideal}}{I} \quad \text{(Equation 4)}$$

$$I = COS + ACOS \; or \; SIN + ASIN \quad \text{(Equation 5)}$$

$$C_{ideal} = \frac{COS - c_C}{a_C} \quad \text{(Equation 6)}$$

$$S_{ideal} = \frac{SIN - c_S}{a_S} \quad \text{(Equation 7)}$$

Since transmittance is physically non-negative, an affine transformation needs to be applied to 'SIN' and 'COS' channel (6, 7) in order to estimate the Cosine and Sine transformation. c_C and c_S are respectively the center value of cosine and sine transmittance profiles (Figure 1A). a_C and a_S are respectively the amplitude of cosine and sine transmittance profiles (Figure 1A). With our specific set of dichroic mirrors, these parameters are $c_C = 0.52$, $c_S = 0.51$, $a_C = 0.44$ and $a_S = 0.40$ (supplemental information).

Sinusoidal dichroic mirror

The two sinusoidal dichroic mirrors are the core components of SHy-Cam. The dichroic mirrors are designed to work in the spectral range of 400nm to 700nm (Figure 1A) as the most commonly used fluorescent proteins and fluorophores emit in the visible spectrum. They have 45-degree angle of incidence and random polarization (Chroma, Inc). The spectral transmittance for the dichroic mirrors closely resembles the shape of a sine and a cosine function, with a maximum transmittance peaking at 95.8% for sine and at 91.1% for cosine, as per manufacturer provided specifications.

Optical design and setup

SHy-Cam presented in this work is designed as a spectral compression add-on device (Figures 1B, S1) to be placed in the infinity space of a custom-built SPIM.[23,24] The SPIM is equipped with multiple single-photon laser lines (404nm, 450nm, 488nm, 561nm and 640nm) which are combined and fill the back focal plane of two oppositely positioned excitation objective lenses (LMPL10XIR, numerical aperture (NA) = 0.25, Olympus). A galvanometer scanner (6215HB, Cambridge Technology) positioned upstream of the excitation objective lenses generates fast scanning spherically focused laser beam along the y direction at the sample, creating a scanned light sheet in the *x-y* plane (Figures S1B and S1C) with 2 μm thickness axially. The scanned light sheet was tuned so that it only illuminates the sample covered by the FoV of SHy-Cam in *y* direction (Figure S1C) to minimize laser-induced phototoxicity. The fluorescence emission was imaged through a 25x water-immersion detection objective lens (CFI75 Apochromat 25XC W, Nikon) which was positioned upstream of the input port of SHy-Cam. SHy-Cam itself can be broken down in two three main sections (Figures 1B, S1A):

Optical filter set: light at wavelengths outside of 400-700nm were rejected by a short-pass filter (FF01-715/SP25, Semrock, Inc) and a long-pass filter (FF01-380/SP25, Semrock, Inc). In addition, we employed a set of notch filters for removing the exciting laser light, centered at 404nm, 488nm, 561nm and 640nm (NF01-488/647-25x5.0; NF03-561E-25, Semrock, Inc.).

Relay lens group: two 2-inch diameter relay lenses RL_1 , RL_2 (32-886, 49-291, Thorlabs, Inc.) and a field stop *FS* (SM1D12C, Thorlabs Inc.). The first relay lens RL_1 creates an intermediate image plane at the field stop. The field stop, a ring-actuated iris diaphragm is adjusted to a size that the final images formed on the sensor do not overlap with each other. The second relay lens re-collimates the light to infinity space.

Image splitter: after the relay lens group, a 50/50 beam splitter *BS* (BSW10R, Thorlabs, Inc) equally divides the fluorescence emission light into two paths. Sine dichroic mirror DM_s and cosine dichroic mirror DM_c (Chroma, Inc.) along with three mirrors RM_{1-3} (CCM1-E02, Thorlabs Inc.) create four spectrally compressed and correlated light paths. Four tube lenses TL_{1-4} (32-884, Edmund Optics) with focal length f =175mm focus the light and form the four-channel final image on a 5MP sCMOS camera sensor (Edge 5.5, PCO, Gmbh). Four mirrors GM_{1-4} (BB1-E02, Thorlabs, Inc.) mounted on gimbal mounts (KC45D, Thorlabs, Inc.) are used in front of the tube lenses to adjust the incidence angles so the images can be formed on the correct locations of the sensor.

All the optical components used in this work can be found from the part list on GitHub repository (Data and Code Availability).

Opto-mechanics

SHy-Cam is built based on both off-the-shelf components (Thorlabs, Inc.) and custom-made 3D printed components with black polylactic acid (PLA) thermal plastic material extruded from an Ender 5 (Creality 3D Technology Co., Ltd) fused deposition modeling 3D printer. The printing nozzle temperature was set to 200 ° C while the print bed was set to 60 ° C for improved adhesion. The layer height was set to 0.2 μm. The 3D printer stepper motors were calibrated on all three axes with rigorous print bed leveling to ensure the dimensional accuracy. All the opto-mechanical components used in this work can be found from the part list on GitHub repository (Code Availability).

Image acquisition

SHy-Cam-SPIM image acquisition

In this work, lasers, sample stages and camera were all controlled by an integrated microscope controlling software called micro-manager.[39,40] The acquisition with SHy-Cam consists of a hybrid registration image for registering four channels, a series of dark frames for removing the background signals and the final fluorescence images of interest.

A hybrid registration image is acquired with both bright-field transmitted illumination and fluorescence excitation with the samples to be examined in place. Bright-field illumination illuminate the whole FoV and the boundaries confined by the field stop (Figure S1) can be observed clearly. Fluorescence excitation provides fluorescent contrast and features within the FoV which will help with the registration step.

The dark frames are acquired using the same settings that are used for final fluorescence images, i.e. the same laser power, same exposure time, same sensor gain and pixel binning. They are acquired continuously for at least 20 frames. During image pre-processing stage, the averaged dark frames is subtracted from the final fluorescence images.

There is no special procedure for the acquisition of final fluorescence images with SHy-Cam equipped with single sCMOS camera (Edge 5.5, PCO, Gmbh). When image tiling is used for covering a larger FoV, the fixed reference channel used for image registration is used to navigate through the sample in 'Multi-Dimensional Acquisition' function in Micro-manager with the sample stage controller. During our test, a proper tile overlapping of 25%-30% was used to achieve good image stitching results. We also use a 2x2 pixel binning during acquisition to enhance SNR and dynamic range.

Confocal image acquisition

We did an imaging comparison test of SHy-Cam-SPIM with a laser scanning confocal microscope (LSM 880, Zeiss) on the same three-color transgenic zebrafish embryo (Figures 2I–2K). We chose the closest combination of laser excitation available on the confocal (488nm, 561nm, 633nm) to match the laser combination used on SHy-Cam-SPIM (488nm, 561nm, 640nm). The ground truth image (Figure 2I) was acquired sequentially with one laser excitation at a time using the 32-channel spectral PMT (410nm-696nm with 8.9nm resolution) with 16-bit bit depth. For each ground truth channel, the intensity value of each pixel was calculated by summing the 32 channels and normalizing the summed value to 16-bit. The hyperspectral image (Figure 2J) was acquired with simultaneous excitation of three laser lines using the 32-channel spectral PMT under the same settings. Both images (Figures 2I and 2J) were acquired using the same 20x objective lens (Plan-Apochromat 20x/0.8 M27, Zeiss). The pinhole was set to 34 μm in order to match the axial resolution of the SPIM.

Image pre-processing

Image registration

SHy-Cam data analysis relies on pixel-wise calculation. Proper registration and alignment of four channels is important and here performed in a three-step process. First, areas on the sensor that respectively correspond to the four channels (Figure S1D), are defined via regions of interest (ROIs) (Code Availability) onto a hybrid registration image acquired with SHy-Cam and serve as reference for later registration.

Second, a set of control points from the four channels is located and used for registration, choosing one channel as the fixed reference, three others as the moving channels to be registered. In this work we use ASIN channel as the reference channel. We performed the registration by using a deformable warping-based image registration method and an ImageJ plug-in software called 'Big Warp' (Figures S1E–S1H).[50] We used the apices of the hexagonal FoV boundaries defined by the 10-blade field stop *FS* (SM1D12C, Thorlabs Inc.) along with 2-3 distinct fluorescence features at the center of the FoV as control points. The registration result can be estimated using the same plug-in software with image overlay visualization (Figures S1E–S1H).

Finally, we utilize a custom MATLAB script (Code Availability) based on local weighted mean registration algorithm[51] to complete the image registration. The script reads the coordinates of rectangular ROI generated in the first step and the control points exported in second step along with the dark frames and fluorescence images of interest during acquisition.

The registered images are saved as OME.TIFF format[52] with the formatting order of (x,y,z,c,t). (x,y,z) is the spatial index. c is the channel index (0: ASIN, 1: ACOS, 2: SIN, 3: COS). t indicates the frame number. The exported images with OME.TIFF format in the described formatting order can be directly imported into analysis software and script (Code Availability).

The first and second step are only required when there is noticeable spatial drifting of any channel. SHy-Cam in this work was built on top of a stabilized optical table (T48H, Thorlabs, Inc.) inside of a temperature-controlled room at 20 $^{\circ}C$. We found the FoV was able to stay within the defined rectangular regions for more than 1 month without adjustment. The control points re-locating on the other hand should be done daily to make sure the registration performance.

Image stitching

SHy-Cam images are first registered using a deformable warping-based image registration method.[50] The registration process utilized one of the four channels as a fixed reference for aligning the other three. For each system physical alignment change, an initial registering process was conducted using the Big Warp plug-in function in Fiji[38] (Figure S1A) to establish the geometrical relations between the reference and registering channels. As long as there is no physical change or misalignment, the registration is performed automatically through a MATLAB script (Code Availability) which uses the previously located control points for registering future data. The registered images are saved as a 4-channel OME-TIFF phasor cube, with layers corresponding to SIN, COS, A-SIN and A-COS (Figure 1B).

In the case of tiled acquisitions (Figures S1I and S1J), image stitching was performed using Imaris Stitcher 9.6 (Bitplane, Switzerland). Results were stored in IMS Imaris file format. For analysis software and script to load the stitched images, a format conversion from IMS to OME.TIFF was done using Imaris 9.7 (Bitplane, Switzerland).

Image analysis

Spectral phasor analysis in HySP

We integrated spectral phasor calculation function into an integrated spectral phasor analysis software previously published HySP (Code Availability).[17] The software reads pre-processed OME.TIF images from the disc and transform each pixel from the original data into phasor coefficients following Equations 3, 4, 5, 6, and 7. The transformed phasor coefficients are then organized into a 2-D histogram for visualization the distribution on the phasor plane (Figures S2A–S2C). Each bin on the phasor plane, the 2-D histogram, corresponds to the pixels from the image with the same spectrum. The separation of multiple fluorescence emissions can be achieved by geometrically applying region of interest masks on the corresponding bins on the phasor plane (Figures 2F, S3A). This 2-D geometric analysis is a fast and intuitive way for the multiplexing purpose for spatially sparse fluorescence and for verifying the existence of certain fluorescence.

In addition, SEER,[25] a spectral phasor-based spectral visualization method was integrated into also HySP. It overlays a specific colormap onto the phasor plane and automatically visualizes the spectral information by mapping the pseudo color from the colormap back to image plane (Figures 2B and 2D).

Ratiometric spectral analysis using spectral linear unmixing

Spectral LU[21,22] can be applied directly to the pre-processed four-channel SHy-Cam image for a quantitative and ratiometric spectral analysis, without spectral phasors conversion. LU is treated as a linear least-squares (LLS) problem which can be represented by Equation 8.

$$\min_{\boldsymbol{x}^n} \frac{1}{2} \| \boldsymbol{R}^{4\times n} \cdot \boldsymbol{c}^n - \boldsymbol{s}^4 \|_2^2 \quad \text{(Equation 8)}$$

$$\boldsymbol{R}^{4\times n} = \left[\boldsymbol{r}^1, \boldsymbol{r}^2 \ldots \boldsymbol{r}^n \right] \quad \text{(Equation 9)}$$

where n is the number of fluorescence signals. $\boldsymbol{R}^{4\times n}$ is a 4-by-n matrix of reference spectra. Each column, $\boldsymbol{r}^k$, of the matrix is a normalized four-channel reference spectra of a pure fluorescence. A custom MATLAB script (Code Availability) loads a pre-processed image and rectangular masks are applied manually and sequentially to the area where contains only a specific pure fluorescence. The pixels inside of each mask are averaged to a four-channel intensity vector $\boldsymbol{I}^k$ which is further normalized by its total intensity $\| \boldsymbol{I}^k \|_1$ and get the reference spectra vector $\boldsymbol{r}^k$. The reference spectra matrix $\boldsymbol{R}^{4\times n}$ is save as a .mat file to be loaded when conducting spectral LU. $\boldsymbol{x}^n$ represents the optimal solution of the contribution vector of n different fluorescence. $\boldsymbol{s}^4$ denotes the normalized four-channel spectral vector from the pre-processed analysis image pixel. $\boldsymbol{I}^n$ is an n-Dimensional identity matrix. $\boldsymbol{J}^n$ is an n-Dimensional all-ones matrix. $\boldsymbol{0}^n$ and $\boldsymbol{1}^n$ are n-Dimensional all-zeros and all-ones vectors. Two constraints are used to better define the problem. The first constraint ensures that the summation of all contributions equals one. The second confines the range of contributions to be zero to one.

Photon-efficiency and -throughput estimation

Photon-efficiency and throughput of five commonly used fluorescence proteins was estimated by summing the light coming out of the four channels at the last surfaces of the tube lenses. The loss along the optical train of SHy-Cam was calculated by considering the photon loss at each optical surface between relay lens RL_1 and the four tube lenses TL_{1-4} into consideration (Figure 1B). All lenses used in the SHy-Cam prototype were MgF_2 coated achromatic lenses (Edmund Optics). The manufacturer-claimed light loss due to reflection is controlled under 1.75%. We used 1.75% as the number to estimate the light loss at the lens surfaces. Spectral specifications of other off-the shelf optical components mentioned above can be found on the respective products webpages. The transmittance and reflectance profiles of two custom sinusoidal dichroic mirrors were provided by manufacturer. The throughput estimation of the filter-based spectral phasor approach[53] was estimated by the average signal of the sine and cosine channel at the last surface of the tube lens.

Sample preparation

Fluorescent dyes

Rhodamine 6G and Rhodamine B powders were respectively dissolved in distilled water to create pure dye solutions with the concentration of 1mg/mL. Five mixtures of the two dye solutions with different relative concentrations (Figures 2B–2D) were created by mixing the two pure dye solutions.

Fluorescent beads

1-μm, 1% solid fluorescent bead samples (L2778 fluorescent red, L1030 fluorescent yellow-green, L9654 fluorescent orange, Sigma-Aldrich; Dragon Green, Flash Red, Suncoast Yellow, Bangs Laboratories, Inc.) were diluted 1000-fold in distilled water, then further

diluted another 100-fold in 1% low-melt agarose. The 10,000-fold diluted fluorescent bead sample in 1% low-melt agarose was pulled into a glass capillary (5-000-1025, Drummond Wiretrol) with a stainless-steel plunger. After the agarose solidified at room temperature at 20 °*C* for 1-2 min, the capillary was transferred to a distilled water-filled imaging chamber and a length of the agarose containing the beads was extruded from the micropipettes allowing optical access.

Transgenic zebrafish embryo

For *in-vivo* imaging tests, zebrafish embryos were immersed in liquid solution of 1% low-melt agarose (made with 30% Danieau solution) and pulled into a glass capillary, and agarose was allowed to solidify at room temperature. The capillary was transferred to a Danieau solution-filled imaging chamber and the agarose containing the embryo was extruded from the micropipettes allowing optical access. 0.075% Tricaine was added to both the agarose solution and Danieau solution-filled imaging chamber to prevent movement of embryos. During imaging, the chamber temperature was set and kept at 28.5 °*C*.

For fixed transgenic zebrafish embryos imaging (Figures 2I–2K), embryos at 4dpf were euthanized with 0.1% tricaine methanesulfate (Sigma-Aldrich Corp.) and then fixed by 4% paraformaldehyde (Sigma-Aldrich Corp.) overnight at 4 °*C*, followed by washing with PBS three times. The embryo to be imaged on Zeiss LSM 780 was immersed in liquid solution of 1% low-melt agarose inside a glass bottom imaging dish. The agarose solidified at the room temperature before transferring the dish onto the microscope stage. Upon finishing the experiment, the fixed embryo was carefully freed from the agarose and got mounted into the glass capillary following the sample mounting procedure for *in-vivo* live embryos, without adding Tricaine.

QUANTIFICATION AND STATISTICAL ANALYSIS

All statistical analyses were performed using MATLAB 2021b (MathWorks, Inc.).

SHy-Cam-SPIM dynamic in-*vivo* imaging photo-bleaching estimation

Sample photo-bleaching during the acquisition of the zebrafish embryo tail-clip wound healing timelapse (Figures 4A–4D, Video S2) and the zebrafish embryo beating heart video (Figures 4E–4H, Video S3) were estimated with normalizing the mean intensity value of the four channels from the last frame by the one from the first frame.

Signal crosstalk analysis of SHy-Cam spectral linear unmixing

The detailed analysis method is described in the legend of Figure S2.

SHy-Cam photon efficiency estimation

The detailed analysis method is described in the legend of Table S1.